Ageing Characterization Under Thermal Test of a Receiver Unit for a Radio Telescope

IEEE INSTRUMENTATION & MEASUREMENT SOCIETY

Received 30 May 2022; revised 4 July 2022; accepted 12 July 2022. Date of publication 25 July 2022; date of current version 2 August 2022.
The review of this article was arranged by Associate Editor G. Tang.

Digital Object Identifier 10.1109/OJIM.2022.3193416

Ageing Characterization Under Thermal Test of a Receiver Unit for a Radio Telescope

MARCANTONIO CATELANI [1] (Member, IEEE), LORENZO CIANI [1] (Senior Member, IEEE), GABRIELE PATRIZI [1] (Member, IEEE), ROBERTO SINGUAROLI [1], JADER MONARI [2], AND FEDERICO PERINI [2]

[1]Department of Information Engineering, University of Florence, 50139 Florence, Italy

[2]INAF-IRA—Northern Cross Radiotelescope, 40059 Villafontana, Italy

CORRESPONDING AUTHOR: L. CIANI (e-mail: lorenzo.ciani@unifi.it)

ABSTRACT The Square Kilometer Array low (SKAlow) is an outstanding project aiming at building the world's largest and most sensitive radio telescope. The Australian Murchison Shire desert has been chosen as location for the low-frequency antennas because of many reasons, such as the atmospheric above the site and the radio quietness due to one of the most remote location worldwide. This location is the optimal choice by a radio astronomy and RF engineering point of views. However, it brings several drawbacks in terms of system availability due to the high temperature conditions that deeply affect the electronics reliability, and the difficulties and the costs associated to maintenance tasks performed in a remote location. Thus, it is fundamental to study the reliability and functional performances of the auxiliary electronic devices in the antennas array using adequate aging tests under temperature stress conditions. The experimental activities carried out in this work allowed to investigate the outbreak of failure mechanisms due to aging and hot temperature conditions in the receiver unit for low-frequency antennas of the SKA project. The experimental results are intended to better determine the strengths and weaknesses of the device under test in order to optimize its installation, its maintenance operations and its functionalities.

INDEX TERMS Antenna arrays, failure analysis, radio astronomy, reliability, temperature control.

I. INTRODUCTION

FAULT diagnosis and reliability analysis are rising research sectors due to the incessant growth and enhancements of electronic, mechatronic and IoT devices [1]–[3]. This is due to the fact that this important revolution comes along with a critical increase of number and variety of failures. Consequently, the electronic system performances are remarkably influenced by such increases in failure mechanisms in terms of reliability and availability point of views. As a matter of fact, the analysis and assessment of component reliability plays a fundamental and critical role during the first phases of the system design [4], [5]. Design for reliability of complex systems is usually carried out following different strategies and implementing different approaches, such as:

- Reliability prediction by means of handbooks that contains failure data of multiple devices. Few examples of common handbooks are the Telcordia SR332-Issue4 published in 2016 for electronic and telecommunication equipment) [6], the Siemens SN29500 for electromechanical and automation devices (last update published in 2013) [7] and the NSWC published in 2011 for mechanical components [8].
- Reliability Importance [9], Reliability Allocation [10] and other analytical models based on Reliability Block Diagram (RBD) [11].
- Markov models, Hidden Markov models [12] and Bayesian networks [13].

The problem with the aforementioned approaches is that they are usually model-based methods. In other words, they rely on analytical models, physical degradation models or simulation scenarios to study the reliability performances of the device.

A valid alternative is played by accelerated aging tests [14], [15], which provides a data-driven approach to study the performances of a system and predict its wear-out behavior by a functional and reliability point of view. Accelerated aging tests allow to achieve information about the component reliability based on the results of tests performed subjecting a product to conditions above the nominal service operations [16], [17].

Environmental stress sources (like high temperature, thermal excursion, high percentage humidity, mechanical shocks, etc.) combined with critical operating conditions (i.e., in terms of high voltage or high current dissipation) are able to trigger failure mechanisms of healthy components in a shorter time than nominal operating conditions (considering both environmental and operating nominal conditions) [18]–[20]. When electronic device reliability become essential in the overall system life cycle management, accelerated aging test are particularly useful because of the following reasons:

- The aging process of electronics is a slow process which takes several years to induce failures. Accelerated aging test uses stressful conditions to speed up the test
- Accelerated aging tests are the only method available in literature to ensure an accurate data-driven functional and reliability analysis under stressful conditions.
- In case of mission-critical and stressful applications in terms of both environmental and functional parameters (few examples are military, aerospace, naval, radio astronomy, nuclear power plant and more generally the electricity production process, and many others) the performance of the device shall not be studied only using analytical and degradation models. In this cases, experimental aging tests allow to collect data that most of the times are not appropriate or even not available in handbooks.

Thus, in this work a functional and reliability analysis of a RF receiver unit for radio astronomy applications has been carried out using a temperature-controlled aging test.

The measurement setup implemented along with the temperature test setup allowed to investigate the appearance, the presence, and the propagation of failure mechanisms due to aging and overheating conditions. The experimental results are intended to better determine the strengths and weaknesses of the device under test in order to optimize its installation, its maintenance operations and its functionalities.

The major contribution of the paper is the introduction of an adequate customized measurement setup for the experimental characterization of the performances and reliability of a receiver unit for the SKA (Square Kilometer Array) project. The results of the proposed test allowed to significantly improve the design of the receiver unit, studying the aging of the device in an operating context similar to the real installation on the field.

II. SYSTEM UNDER ANALYSIS

A. THE SKA PROJECT

The Square Kilometer Array (SKA) [21] project is an international organization aiming to build the most large and sensitive radio telescope in the world. In order to do that, a signal collection area of over 1 km^2 has been considered representing an outstanding step toward the design and implementation of a unique instrument for radio astronomy purposes [22].

The SKA project comprises hundreds of high-frequency dish type antennas (0.35 - 15.5 GHz) deployed in South Africa's Karoo region along with a thousands low-frequency antennas (50 - 350 MHz) installed in Western Australia's Murchison Shire desert [23].

Due to size and complexity of the SKA project, it required a fragmentation of the work into different phases. The first step consists of the development of a demonstrator (Aperture Array Verification System, AAVS1) of 256 low-frequency antennas located in the Murchison Shire region. AAVS1 is the first of multiple prototype installations whit the aim of demonstrate and evaluate potential telescope design solutions [24].

Each station of 256 antennas is called LFAA (Low-Frequency Aperture Array) and it represents the objective of this work. LFAA will then constitute a part of the future overall antennas array (called SKA1-low), consisting of 512 LFAA stations. Since each LFAA is composed by 256 antennas, the entire SKA1-low will reach a total of over 130'000 antennas. Then, in the following phases, the number of total antennas is expected to reach up to 1 million [25].

The distribution of the antennas of the SKA project follows a particular geometry, where 75% of the devices are concentrated in a small central area characterized by a diameter of 2 km, while the remaining 15% of theme is distributed over 3 spiral arms reaching up to 75 km away from the center of the geometry. Using such deployment of the antenna is possible to achieve high resolution while ensuring the level of the secondary lobes as low as possible.

B. GENERAL SYSTEM ARCHITECTURE

The SKALA2 antennas included in the AAVS1 project works in double polarization (horizontal and vertical) in the 50 MHz $\div$ 650 MHz band.

Considering an individual AAVS1 station, the antennas are grouped into cells (also known as tiles) of 16 antennas. Each tile therefore generates a total of 32 signals (due to the double polarization of each antenna) which is adequately preprocessed, and then digitized and combined to generate several beams. The various beams coming out from the 16 tiles are combined together in order to obtain a single beam for each one of the stations. Subsequently, a correlator system operates to correlate all the beams of all the stations, creating the overall response of the entire array.

The signals detected by the antenna are amplified by two differential Low Noise Amplifiers (LNA) placed at the top

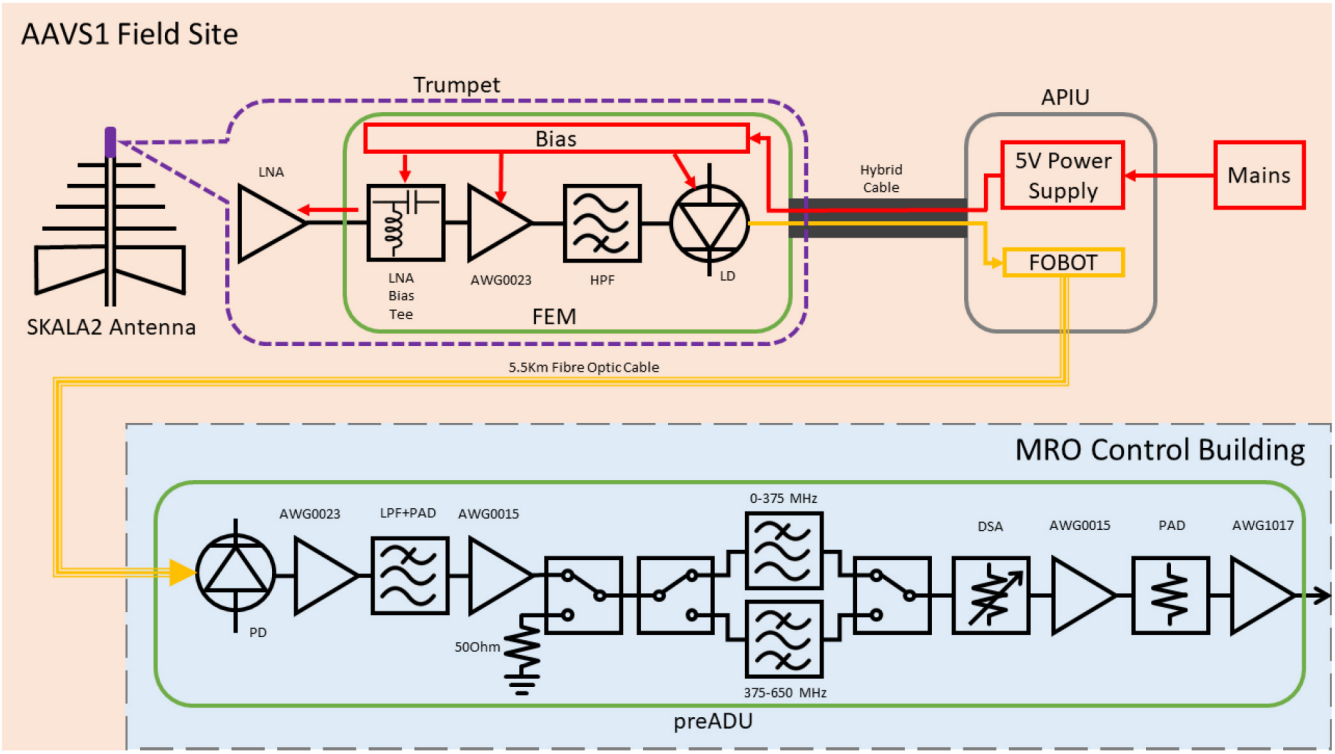

FIGURE 1. Schematic representation of the acquisition chain contained in a single tile identifying three main blocks: antenna & LNA, receiver, signal processing.

of each antenna. The two signals are then processed by the following block, called Front End (FE). The FE generates a single amplified RF signal which is then converted into optical signal by means of an electrical-optical conversion unit to allow easy and robust data transmission via analog fiber optic. The optical signal reaches a TPM (Tile Processing Module) system, which is processing device basically composed by a PRE-ADU block and an ADU block (where the abbreviation ADU stands for Analog to Digital Unit) [26]. The entire system is illustrated in a schematic block diagram in Fig. 1.

C. THE DEVICE UNDER TEST

In this activity the AAVS1 Front End block (SN F-040/201611) has been tested. The device is a component of the radio frequency receiver chain located on top of the receiving antenna, which is arranged vertically on the ground, as it is possible to see in Fig. 2. The reception frequency of the signals falls within the 50 MHz ÷ 650 MHz band. The two signals received by the antenna (related to the horizontal and vertical polarization components) are preprocessed by two LNA before becoming the input signal of the FE under test. The tested Front-End elaborates and adapts the two received signals by means of the WDM (Wavelength-Division Multiplexing) technique to ensure that both signals can be transmitted on a unique single-mode optical fiber.

The optical fiber connects the top of the antenna with the remote receiving unit located in the control room. A photo

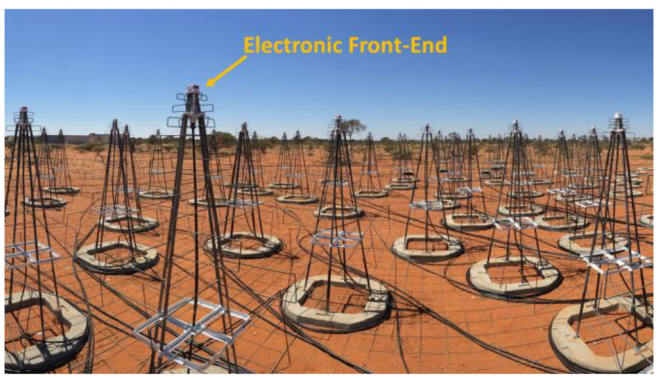

FIGURE 2. Picture of the antennas included in the AAVSI installation highlighting the positioning of the FE.

of the device under test before starting the test procedure is shown in Fig. 3. The electronics are enclosed in a protective plastic casing, called trumpet.

Due to the installation constraints, the electronic devices included in the FE must endure critical environmental conditions in terms of thermal stress (due to solar radiation) and component overheating (i.e., an additional temperature rise due to additional power dissipation).

Along with these problems, it is important to take into account the difficulties and the costs associated to maintenance tasks performed in a remote location such as the Australian's Murchison Shire desert.

FIGURE 3. The AAVS1 Front-End device (on the right side of the picture) connected to the wavelength division multiplexer (on the left side of the picture) during the characterization performed before the test session.

III. DEVELOPMENT OF THE AGING TEST

A. TEST PLAN

According to the operational data collected during the prototype phase, a thermal aging test has been proposed for the FE device under test. The device, and part of the monitoring instrumentation, have been provided by the Italian National Institute for Radio Astronomy and Astrophysics INAF-IRA.

The severity of the test in terms of both duration and temperature has been studied considering the major criticalities arisen in the project. Particular attention has been paid to the optical components (laser diodes driving the optical fiber). In this case, the operating temperature characteristics of the application field significantly affect the system performances, strongly limiting the driving current and the optical power [27], [28].

Thus, the testing temperature has been set equal to 80 °C in order to stress the endurance of the device inducing an accelerated aging without causing critical failure due to excessive overstress.

Furthermore, the proposed high temperature condition allows to overstate the excessively heat operating context that characterize the environment of installation in the Western Australia's Murchison Shire desert. Overall, a testing temperature of 80 °C is the optimal choice to age the device under operating conditions even worse than the ones that characterize the actual installation, without trigger any destructive failure mechanisms.

To be thorough, a brief note regarding negative temperature conditions is required. Testing the device at a cold temperature condition is not reasonable and not significant of the actual operating context in which the receiver unit is installed. Furthermore, cold temperature has a minor effect on the aging of electronic devices. These are the reasons that lead this research only toward hot temperature, neglecting cold temperature.

The severity of the proposed test plan is summarized in Table 1, while a schematic representation of the test profile is shown in Fig. 4.

A preliminary characterization phase (called pretest phase in Fig. 4) is required in order to characterize the device under nominal operating conditions. This phase is performed at ambient temperature (T_{amb} = 20 °C) to ensure the acquisition of sufficient amount of data regarding the standard working operations of the DUT. After that, temperature must be increased from T_{amb} up to T_H = 80 °C with a controlled increase rate of 1 °C/min (Rise time phase in Fig. 4). The actual aging test begins once the exposition temperature T_H is reached. This phase called test execution lasts 800 h. Finally, a fall time phase performed decreasing temperature at 1°C/min allows to reach again the ambient temperature before carrying out the final characterization of the test.

This final phase is performed in standard operating condition, after that the external temperature stress has been removed.

TABLE 1. Severity of the proposed thermal aging test.

Type of test	Thermal aging
Exposition temperature	T_H = 80 °C
Test duration	800 h
Test requirements	DUT powered and properly working during the entire test
Test points	Intermediate control at 400 h and 600 h

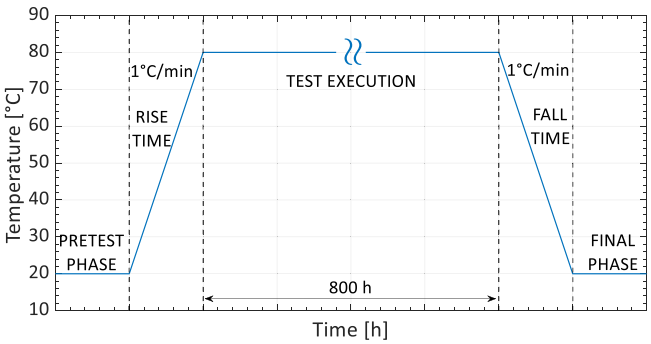

FIGURE 4. Structure of the proposed temperature test plan.

B. FAILURE CRITERIA

Measurements of DC power consumption and RF parameters (Input and Output return losses, Gain, Gain Flatness, Band Shape, Noise Figure, P1dB compression point and IP2/IP3) are carried out before (pretest phase in Fig. 4) and after (final phase in Fig. 4) the test execution.

In this way it is possible to analyze the data acquired in standard condition and verify if any electrical malfunction caused by temperature has occurred during the test execution.

IV. EXPERIMENTAL SETUP

In order to implement the proposed test plan, a suitable experimental setup has been designed and developed. The aim of the measurement setup is to expose the DUT to thermal stress and, at the same time, to acquire data regarding the health state and the correct functioning of the device.

TABLE 2. Summary of devices used to implement the aging test for the characterization of the DUT.

LABEL	DEVICE	MODEL/DESCRIPTION
#1	Thermal chamber	ISCO S2A00005-NSC9120
#2	Data Acquisition System	Agilent 34970A equipped with Agilent 34902A - 16 channel multiplexer
#3	Data acquisition Software	Agilent Bench-Link®
#4	Thermocouples	N-type (monitoring DUT surface, temperature around DUT and ambient temperature)
#5	Optical Power meter	Fotec m (899493)
#6	WDM optical splitter	FWDM-1X2-1270P/1330R-2000-1-1-NE-90X16X9
#7	Digital Multimeter	HP 34401A
#8	Power supply	MCP Triple output adjustable power supply
#9	Storage device	Laptop

A summary of all the devices required to implement the test is included in Table 2. The DUT has been placed in the middle plane of a thermal chamber (Test equipment #1), connected to the power supply source (Test equipment #8). The selected supply required for the proper functioning of the DUT is 5 VDC.

An adequate set of N-type thermocouples (Test equipment # 4) has been placed on the top surface and around the DUT in order to acquire data regarding the device overheating and the ambient temperature. The time-interval for the acquisition data system has been set equal to 1 min during the rise (from up $T_{amb} = 20$ °C to $T_H = 80$ °C) and fall (from $T_H = 80$ °C to $T_{amb} = 20$ °C) phases. Instead, during the thermal stress exposure at T_H the data acquisition system (Test equipment #2) has been set to acquire data with a time-interval of 15 min. The sink current has been measured by a digital multimeter (Test equipment # 7). The output optical power has been acquired by a dedicated customer equipment (Test equipment #5 and Test equipment #6).

A picture of the complete experimental setup is illustrated in Fig. 5 including labels identifying the different devices according to Table 2. A detail of the optical power measurement (Test equipment #5 and Test equipment #6) is reported in Fig. 6, while Fig. 7 shows the DUT placed inside the thermal chamber.

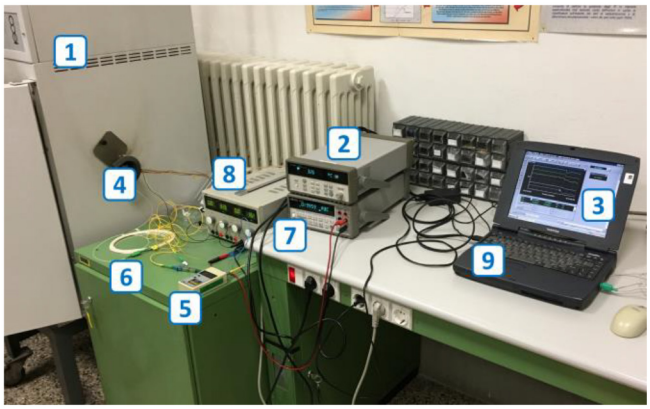

FIGURE 5. Picture of the experimental setup highlighting all the devices. The numeric labels refer to the device classification a in Table 2.

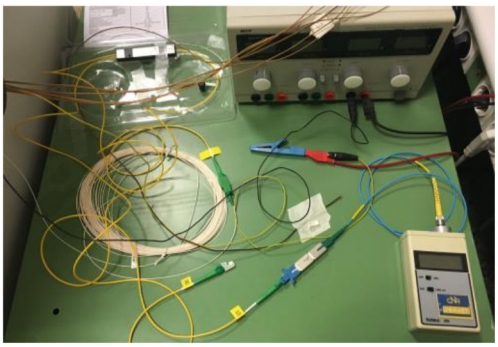

FIGURE 6. Measurement setup dedicated to the optical power acquisition.

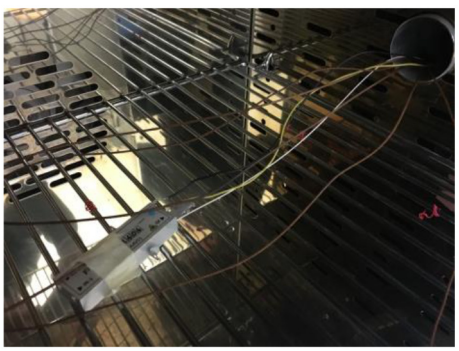

FIGURE 7. Detail of the DUT placed inside the thermal chamber and installation of the monitoring thermocouples.

V. EXPERIMENTAL RESULTS

The aging test carried out in this work can be divided into three separated phases:

1) Rise phase - the chamber temperature passes from ambient temperature to $T_H = 80$ ° C according to Section III. Temperature variation is performed at slow rate to ensure a gradual heating of the device.
2) Test execution (exposure phase) - it starts when temperature stability at $T_H = 80$ ° C has been reached. The chamber temperature is set and automatically controlled to maintain temperature constant. This is the actual aging phase of the test, and it involves two intermediate checks at 400 h and 600 h to verify the correct functioning of the DUT.
3) Fall phase - the DUT is brought back to room temperature. Temperature variation is performed at slow

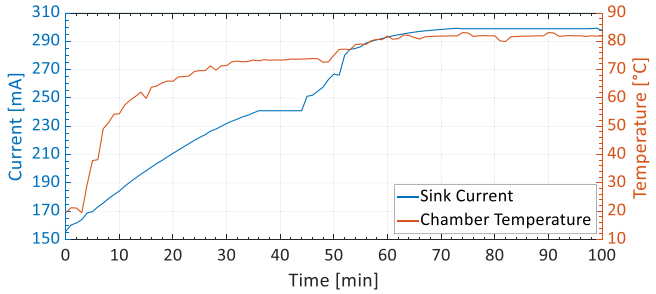

FIGURE 8. Sink current of the DUT measured during the rise phase of the test (left Y-axis) compared with chamber temperature (right Y-axis).

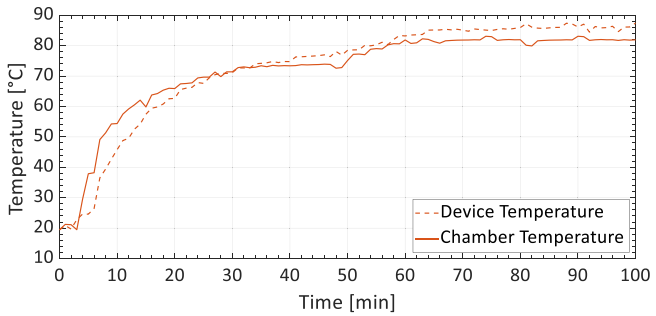

FIGURE 9. Temperature trend during the rise phase of the test: device temperature (dashed line) against chamber temperature (solid line).

rate to ensure a gradual cooling of the device avoiding failure due to thermal shock.

During each phase, the temperatures, the sink current and the optical power are automatically acquired using the measurement set-up as described in Section IV. The measurements of the above-mentioned parameters are repeated considering two different wavelengths that could be managed by the Front-End under test during actual working conditions (i.e., $\lambda_1 = 1270$ nm and $\lambda_2 = 1330$ nm). The two wavelengths are transmitted at the same time along the optical fiber, according to the technical constraints of the entire AAVS1 stations. The external WDM optical splitter selects the wavelengths, and it allows to feed separately on the optical power meter instrument the two different signals. During the pretest measurement at ambient temperature the optical power measured in case of both wavelength λ_1 and λ_2 varies in the range from 3.87 dBm to 4.68 dBm. In the same condition, a sink current of 155 mA has been measured by the dedicated setup. During the rise phase the sink current increases constantly until it reaches approximately 300 mA when temperature inside the chamber reaches $T_H = 80$ ° C. The detail of the absorbed current during the rise phase are shown in Fig. 8. The figure clearly highlights a significant dependency between the sink current and the temperature. When temperature stability has been reached, also current stability can be obtained. This current gradient caused by the temperature dependance of the device lead to an increase of the device's temperature that has been monitored and illustrated in Fig. 9. Under standard operating conditions (pretest phase, sink current of

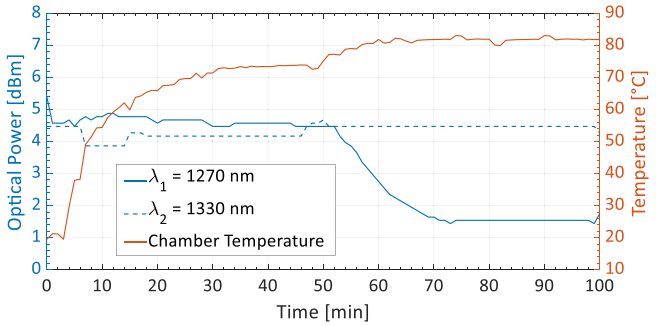

FIGURE 10. Optical power measured during the rise phase considering two allowed wavelengths: $\lambda_1 = 1270$ nm (solid blue line) and $\lambda_2 = 1330$ nm (dashed blue line).

approximately 155 mA) device and ambient are under thermal equilibrium. During the initial steps of the rise phase ambient temperature increases, however device temperature increment proceeds slower due to thermal inertial. However, when temperature stability at $T_H = 80$ ° C is reached within the chamber, then device temperature continues to increase due to the growth of the sink current. Overall, this leads to a component overheating of approximately 5 °C. When the device will be installed in the dedicated deployment in the Australian Murchison Shire desert, the ambient temperature could realistically reach extremely high values. This will lead to a significant current consumption and remarkably high device's temperature which could severely affect the system reliability. The proposed test allowed to discover this problem, and thus to predict the impact that a possible excessive heating will have on the probability that the Front-End will fail.

Fig. 10 shows the optical power for the considered wavelengths as a function of temperature during rise phase. The optical power measured for the wavelength $\lambda_2 = 1330$ nm still remains within the range from 3.87 dBm to 4.68 dBm during the entire rise phase. The device overheating does not influence the optical power of this configuration, as well as the measured values remains approximately constant even during the 800 h of exposition phase at $T_H = 80$ ° C.

Quite the contrary, there is a significant variation of the optical power measured considering the wavelength $\lambda_1 = 1270$ nm. When temperature overcomes approximately 50 °C the optical power decreases until it stabilizes around +1.5 dBm.

Basically, considering the 1270 nm acquisition channel, the constant overcurrent caused by the DUT's heating lead to a decrease of the optical power because of the LDO (Low-dropout regulator) included in the internal power supply of the FE. In fact, in case of high current condition the LDO enters in a self-limitation state, and it no longer supplies the necessary current to maintain constant the optical power. This behavior is illustrated in Fig. 11 where the optical power (only in case of $\lambda_1 = 1270$ nm) and the sink current during the rise phase are shown.

At exposure temperature of T_H (actual aging of the DUT) the measured optical power for the λ_1 wavelength is in the

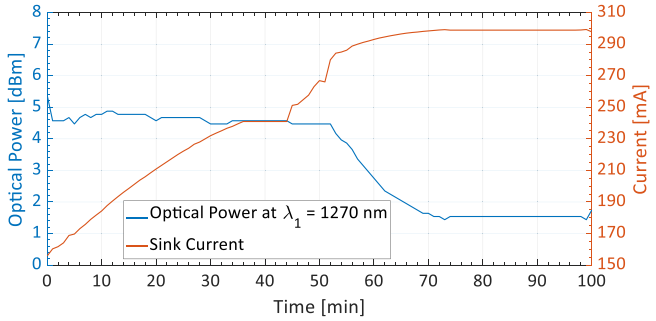

FIGURE 11. Trend of the optical power for the channel at 1270 nm compared with the current absorbed by the FE as a function of time during the rise phase of the test.

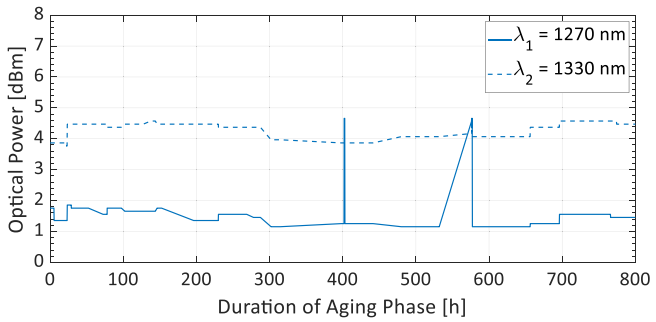

FIGURE 12. Optical power measured during the exposition time at 80 °C (aging phase of the test).

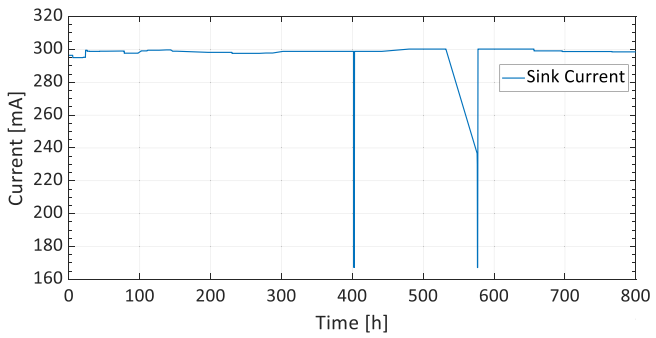

FIGURE 13. Sink current measured during the exposition time at 80 °C (aging phase of the test).

range 0.95 ÷ 1.76 dBm (−3 dB loss respect to standard operating conditions), while the measured optical power for the λ_2 wavelength remains permanently within the range 3.87 ÷ 4.68 dBm (no loss respect to standard conditions).

The complete aging phase (in terms of optical power) is shown in Fig. 12, where the solid line stands for the optical channel working at λ_1, while the dashed line represents the optical channel working at λ_2. Instead, the trend of the sink current during the aging phase is illustrated in Fig. 13. Analyzing both Fig. 12 and Fig. 13 it is possible to note two spikes in the sink current (Fig. 13) and two spikes in the optical power of the λ_1 channel (solid line in Fig. 12).

In both figures, the spikes are in correspondence with the two intermediate inspection phases set after 400 h and 600 h. During these inspections, the temperature of the climatic

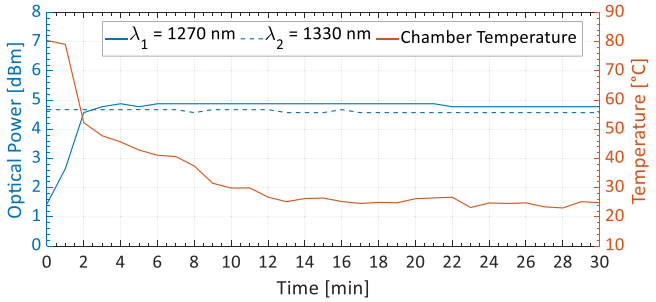

FIGURE 14. Optical power measured during the final cooling phase considering $\lambda_1 = 1270$ nm (solid blue line) and $\lambda_2 = 1330$ nm (dashed blue line).

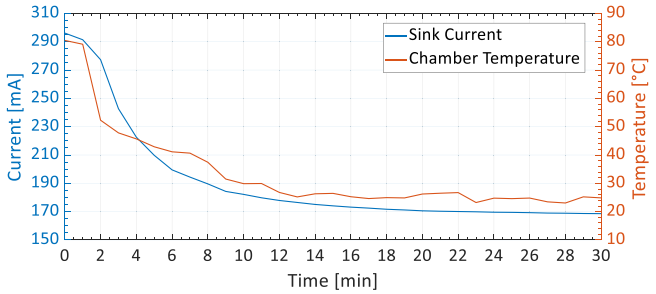

FIGURE 15. Sink current of the DUT measured during the final cooling phase of the test (left Y-axis) compared with chamber temperature (right Y-axis).

chamber is lowered from T_H to ambient temperature to allow a proper analysis of the device's health status. The inspections confirmed the proper working of the device and proved that no failure mechanisms have been triggered by the test neither after 400 h, nor after 600 h. Kin fact, during the inspections, the performance of the receiver unit under analysis return back to the original values acquired at standard operating conditions before the test. The decrease of the sink current due to the lowering phase of the test temperature led to a temporary increase of the optical power, which then goes back to the low values around +1.5 dBm when the test starts again.

The final analysis deals with the characterization during the final cooling phase (fall phase) of the test. Fig. 14 shows the trend of the optical power measured during this phase. To confirm what is shown in Fig. 11, the optical power of the channel at $\lambda_1 = 1270$ nm returns to the initial values similar to those measured for the channel at $\lambda_2 = 1330$ nm.

Similarly, also the sink current returns to the initial levels around approximately 170 mA as soon as the test temperature decreases reaching the ambient condition (see Fig. 15). This result is extremely important for the characterization of the device. As a matter of fact, the decrease of the optical power of the channel at $\lambda_1 = 1270$ nm, as well as the additional current flow and the excessive temperature rise could be interpreted as a symptom of a failed components.

However, since all the parameters return back to their original status when temperature is lowered to ambient condition, it is possible to conclude that the test has induced only an accelerated aging, without triggering any failure mechanisms.

VI. CONCLUSION

The research activity carried out in this work falls within the context of "design for reliability" and uses measures to optimize and ensure adequate reliability through specific tests, diagnostics and monitoring of complex systems.

In particular, the thermal aging test performed in this work has been passed by the device under test without any failure induced by the stress test. In fact, after the 800 h of thermal aging tests, the Front-End is still properly functioning. The major criticalities arisen during the aging of the receiver unit under analysis are an increment in the sink current absorbed by the DUT, together with a decrease of the optical power of one of the two channels. This is due to the operating temperature that, once a certain threshold has been reached (approximately 50 °C), lead some part of the electronic FE in a self-limitation state. Thus, the test significantly helps to improve the design of the receiver since such phenomenon cannot be neglected due to the zone of the final installation. The discoveries also allowed to verify the correct sizing of the components included in the Front-End, with particular attention to the LDO (Low-dropout regulator).

Finally, the problems that emerged during the proposed test will led to a specific survey of temperature measurements on the final installation site in the Australian desert.

REFERENCES

[1] N. Huang, Q. Chen, G. Cai, D. Xu, L. Zhang, and W. Zhao, "Fault diagnosis of bearing in wind turbine gearbox under actual operating conditions driven by limited data with noise labels," *IEEE Trans. Instrum. Meas.*, vol. 70, pp. 1–10, 2021.

[2] M. Catelani, L. Ciani, D. Galar, and G. Patrizi, "Risk assessment of a wind turbine: A new FMECA-based tool with RPN threshold estimation," *IEEE Access*, vol. 8, pp. 20181–20190, 2020.

[3] S. Keshani, N. Masoumi, and S. Safavi-Naeini, "Reliable, intelligent, and design-independent digital frequency extraction methodology for high bit-count DIFM receivers," *IEEE Trans. Instrum. Meas.*, vol. 70, pp. 1–12, 2021.

[4] M. Catelani, L. Ciani, G. Patrizi, and M. Venzi, "Reliability allocation assessment using MEOWA method in complex redundant systems," in *Proc. IEEE Int. Symp. Syst. Eng. (ISSE)*, Oct. 2016, pp. 1–5.

[5] R. Reis, G. Wirth, and Y. Cao, *Circuit Design for Reliability*. New York, NY, USA: Springer, 2015.

[6] "Reliability prediction procedure for electronic equipment," Telcordia Netw. Infrastruct. Solutions (NIS), Bridgewater, NJ, USA, Telcordia document SR-332, 2016.

[7] *Failure Rates of Components*, Siemens Standard SN 29500, 2013.

[8] *Handbook of Reliability Prediction Procedures for Mechanical Equipment*, NSWC, Washington, DC, USA, May 2011.

[9] Y. Du, S. Si, and T. Jin, "Reliability importance measures for network based on failure counting process," *IEEE Trans. Rel.*, vol. 68, no. 1, pp. 267–279, Mar. 2019.

[10] M. Catelani, L. Ciani, G. Guidi, and G. Patrizi, "Reliability allocation: An iterative approach for complex systems," in *Proc. IEEE Int. Symp. Syst. Eng. (ISSE)*, 2021, pp. 1–6.

[11] M. Sahinoglu and C. V. Ramamoorthy, "RBD tools using compression, decompression, hybrid techniques to code, decode, and compute reliability in simple and complex embedded systems," *IEEE Trans. Instrum. Meas.*, vol. 54, no. 5, pp. 1789–1799, Oct. 2005.

[12] P. Arpaia *et al.*, "Fault detection on fluid machinery using hidden Markov models," *Measurement*, vol. 151, Feb. 2020, Art. no. 107126.

[13] M. S. Ibrahim *et al.*, "System level reliability assessment for high power light-emitting diode lamp based on a Bayesian network method," *Measurement*, vol. 176, May 2021, Art. no. 109191.

[14] J. J. Ruan *et al.*, "An accelerated stress test method for electrostatically driven MEMS devices," *IEEE Trans. Instrum. Meas.*, vol. 61, no. 2, pp. 456–461, Feb. 2012.

[15] H. Liu, T. Claeys, D. Pissoort, and G. A. E. Vandenbosch, "Prediction of capacitor's accelerated aging based on advanced measurements and deep neural network techniques," *IEEE Trans. Instrum. Meas.*, vol. 69, no. 11, pp. 9019–9027, Nov. 2020.

[16] M. Catelani, L. Ciani, G. Guidi, and G. Patrizi, "Accelerated testing and reliability estimation of electronic boards for automotive applications," in *Proc. IEEE Int. Workshop Metrol. Autom. (MetroAutomotive)*, Jul. 2021, pp. 199–204.

[17] M. Catelani, L. Ciani, G. Guidi, and M. Venzi, "Parameter estimation methods for failure rate distributions," in *Proc. 14th IMEKO TC10 Workshop Tech. Diagn. New Perspect. Meas. Tools Techn. Syst. Rel. Maintainability Safety*, 2016, pp. 441–445.

[18] *Semiconductor Devices—Mechanical and Climatic Test Methods—Part 23: High Temperature Operating Life*, Standard IEC 60749-23, 2004.

[19] W. B. Nelson, *Accelerated Testing—Statistical Models, Test Plans, and Data Analysis*, 2nd ed. New York, NY, USA: Wiley, 2004.

[20] M. F. Zakaria, Z. A. Kassim, M. P.-L. Ooi, and S. Demidenko, "Reducing burn-in time through high-voltage stress test and Weibull statistical analysis," *IEEE Design Test Comput.*, vol. 23, no. 2, pp. 88–98, Mar./Apr. 2006.

[21] "SKA Project Official Website." SKA Organisation. [Online]. Available: https://www.skatelescope.org/ (Accessed: May 20, 2022).

[22] S. J. Tingay, "An overviewof the SKA project: Why take on this signal processing challenge?" in *Proc. IEEE Int. Conf. Acoust. Speech Signal Process. (ICASSP)*, Apr. 2015, pp. 5640–5644.

[23] P. Bolli *et al.*, "Test-driven design of an active dual-polarized log-periodic antenna for the square kilometre array," *IEEE Open J. Antennas Propag.*, vol. 1, pp. 253–263, 2020.

[24] P. J. Hall, P. Benthem, and A. T. Sutinjo, "Aperture array verification system 1: Overview of a square kilometre array prototype," in *Proc. Int. Conf. Electromagn. Adv. Appl. (ICEAA)*, Sep. 2016, pp. 345–348.

[25] D. B. Davidson *et al.*, "Electromagnetic modelling of the SKA-LOW AAVS1.5 prototype," in *Proc. Int. Conf. Electromagn. Adv. Appl. (ICEAA)*, Sep. 2019, pp. 1032–1037.

[26] J. Nanni *et al.*, "Challenges due to rayleigh backscattering in radio over fibre links for the square kilometre array radio-telescope," in *Proc. 21st Int. Conf. Transparent Opt. Netw. (ICTON)*, Jul. 2019, pp. 1–4.

[27] L. A. Johnson, "Laser diode burn-in and reliability testing," *IEEE Commun. Mag.*, vol. 44, no. 2, pp. 4–7, Feb. 2006.

[28] E. Suhir, Y. C. Lee, and C. P. Wong, *Micro- and Opto-Electronic Materials and Structures: Physics, Mechanics, Design, Reliability, Packaging*. New York, NY, USA: Springer, 2007.

MARCANTONIO CATELANI (Member, IEEE) received the M.S. degree in electronic engineering from the University of Florence, Florence, Italy, in 1984, where he is currently with the Department of Information Engineering. Strictly correlated with reliability, availability, maintainability and safety (RAMS) are the fields of interest of both the fault diagnosis and reliability testing for components and equipment. In particular, the research activity concerns the development of test profiles used both for the characterization and the evaluation of reliability performance and, at the same time, the development of new degradation models able to estimate the life cycle of electronic components. His current research interests include development of automatic measurement system, the characterization of A/D converters, quality control and related statistical methods, and RAMS context.

LORENZO CIANI (Senior Member, IEEE) received the M.S. degree in electronic engineering and the Ph.D. degree in industrial and reliability engineering from the University of Florence, Florence, Italy, in 2005 and 2009, respectively, where he is currently an Associate Professor with the Department of Information Engineering. He has authored or coauthored more than 160 peer-reviewed journal and conference papers. His current research interests include system reliability, availability, maintainability and safety, reliability evaluation test and analysis for electronic systems and devices, fault detection and diagnosis, and electrical and electronic instrumentation and measurement. He received the 2015 IEEE I&M Outstanding Young Engineer Award for "his contribution to the advancement of instrumentation and measurement in the field of reliability analysis." He is an Associate Editor of the IEEE ACCESS and an Associate Editor-in-Chief of the IEEE TRANSACTION ON INSTRUMENTATION AND MEASUREMENT. He is a member of the IEEE IMS TC-32 Fault Tolerant Measurement Systems.

GABRIELE PATRIZI (Member, IEEE) received the bachelor's degree *(cum laude)* in electronic and telecommunications engineering, the master's degree *(cum laude)* in electronic engineering, and the Ph.D. degree in industrial and reliability engineering from the University of Florence, Italy, in 2015, 2018, and 2022, respectively, where he is currently a Postdoctral Research Fellow of Instrumentation and Measurement and an Adjunct Lecturer of Electric Measurements. His research interests include life cycle reliability of complex systems, condition monitoring for fault diagnosis of electronics, safety instrumented systems, data-driven prognostic, and health management.

ROBERTO SINGUAROLI works with the Department of Information Engineering, University of Florence, Italy, where he holds a job in electronic engineering, RAMS, and quality assurance engineering. He is currently a Technical Manager of the Electrical Engineering and Measurements Laboratory, as a Technical Manager of Testing for Reliability (UNIFI-ANALYTICAL Joint Lab), Technical Reviewer in environmental testing. He collaborates with ACCREDIA—The Italian Accreditation Body—as a Technical Assessor.

JADER MONARI received the degree in electronic engineering from the University of Bologna in 1996. In 2004, he started a collaboration within Square Kilometer Design Studies. In particular, he worked with the design of BEST receiver architecture (Italian Test Bed for SKA) and for the EMBRACE receiver (Dutch SKA Pathfinder Planar Aperture Array). He has been a member of the PREPSKA Team since 2008, as a Liaison Engineer, and he became a Program Coordinator for Italian AAlow task apart of the Aperture Array Verification Program (AAVP Program) then became Aperture Array Design Consortia (AADC). Within AADC, he was appointed as a Task Leader for receivers. He is an Italian Program Manager for all SKAlow tasks and, at an international level, part of the Executive Board that coordinates all the activities of this phase. He is also part of the SKA and LOFAR Italian Board appointed by the Scientific Directorate. He has been a Medicina Radiotelescope Station Manager since nine years.

FEDERICO PERINI received the Laurea degree in telecommunications engineering from the University of Bologna in 2001. Since 2002, he has been working with IRA/INAF with the Medicina Radio Observatory. His expertise covers LNA, RF/IF receivers, and RFoF systems designed and developed for the Italian Radio Telescopes (Northern Cross Array, VLBI dishes of Medicina and Noto, and the Sardinia Radio Telescope) and for international low-frequency instruments as LOFAR2.0, and the forthcoming SKA-Low.